

Beamforming Design for Intelligent Reflecting Surface Aided Near-Field THz Communications

Chi Qiu, Qingqing Wu, Wen Chen, Meng Hua, Wanming Hao, Mengnan Jian, Fen Hou

Abstract—Intelligent reflecting surface (IRS) operating in the terahertz (THz) band has recently gained considerable interest due to its high spectrum bandwidth. Due to the exploitation of large scale of IRS, there is a high probability that the transceivers will be situated within the near-field region of the IRS. Thus, the near-field beam split effect poses a major challenge for the design of wideband IRS beamforming, which causes the radiation beam to deviate from its intended location, leading to significant gain losses and limiting the efficient use of available bandwidths. While delay-based IRS has emerged as a potential solution, current beamforming schemes generally assume unbounded range time delays (TDs). In this letter, we first investigate the near-field beam split issue at the IRS. Then, we extend the piece-wise far-field model to the IRS, based on which, a double-layer delta-delay (DLDD) IRS beamforming scheme is proposed. Specifically, we employ an element-grouping strategy and the TD imposed on each sub-surface of IRS is achieved by a series of TD modules. This method significantly reduces the required range of TDs. Numerical results show that the proposed DLDD IRS beamforming scheme can effectively mitigate the near-field beam split and achieve near-optimal performance.

Index Terms—IRS, THz, near-field, and beam split.

I. INTRODUCTION

Terahertz (THz) communication is a promising technique for future sixth-generation (6G) wireless communications due to its ultra-wide bandwidth, which is expected to achieve data rates of up to terabits per second (Tb/s) theoretically [1]. However, THz signals face significant challenges, including severe transmission attenuation and poor scattering, which limits the transmission range. Fortunately, intelligent reflecting surface (IRS) is a promising solution to these challenges. By using a large number of passive reflection elements, an IRS can steer the signals to any desired direction [2], [3]. This capability allows the IRS to enhance signal strength, making it a practical solution for future THz communications [4].

Although significant efforts have been made, most existing IRS beamforming schemes do not perform well when the signal bandwidth is large, especially in practical THz communication systems. This is primarily because practical IRS is usually equipped with frequency-independent phase-shifting circuits [2], resulting in IRS-aided communications only being able to

achieve frequency-independent beamforming. This leads to the beam split issue in the IRS-aided THz system. In [5], a delay-adjustable metasurface was proposed, where each IRS element is connected to a time-delay (TD) module. The beam split effect could be addressed because the imposed delay enabled frequency-dependent IRS beamforming. However, since the number of IRS elements required in THz scenarios is relatively huge, equipping each element with a TD module becomes impractical, leading to excessive hardware cost and power consumption. In both [6] and [7], the delay-based IRS was designed in a sub-connected manner. The above works only addressed the far-field beam split effect. In fact, due to the high propagation losses and the short wavelength, a THz IRS is expected to consist of a massive number of passive reflecting elements, making the transceivers very likely located in the near-field region of the IRS. Although [8] proposed a delay-based solution to overcome the near-field beam split effect at the IRS, the required number of TD modules was still large and it also ignored the practical limitation of TD technology in the THz band. In fact, research on TD realization in the THz band is still in its early stages, with a limited achievable delay range. Specifically, the TD module discussed in [9] was only able to achieve a maximum delay range of 14.272 picoseconds (ps). Given this limitation, it is crucial to take into account the practical THz TD capabilities when designing the delay-based IRS.

Motivated by the delta-delay-phase precoding proposed in [10] that effectively reduces the maximum range of TD modules, we propose a delay-based IRS beamforming to overcome the aforementioned near-field beam split challenge in this letter. By extending the piece-wise far-field model in [11] to the uniform planar array (UPA) structured IRS, we divide the IRS into multiple sub-surfaces, each of which is imposed by a same TD value, and reasonably assume that the BS and the user are in the far-field range of each small sub-surface. This partition enables us to decompose the phase difference among different IRS elements that causes beam split into two separate components, i.e., the inter-surface phase difference and the intra-surface phase difference. To alleviate the inter-surface phase discrepancy, we propose a double-layer delta-delay (DLDD) architecture. In this design, the first layer TD network takes care of the phase discrepancy along one axis of IRS, while the second layer takes care of that along the other axis. Numerical results reveal the necessity of delay-enabled frequency-dependent IRS beamforming and demonstrate the effectiveness of the proposed scheme in mitigating the near-field beam split effect. Furthermore, it shows that the proposed DLDD IRS beamforming scheme can achieve near-optimal performance using short-range practical TD modules.

C. Qiu and F. Hou are with the State Key Laboratory of Internet of Things for Smart City and the Department of Electrical and Computer Engineering, University of Macau, Macau SAR, 999078, China (e-mail: yc17434@connect.um.edu.mo; fenhou@um.edu.mo). Q. Wu and W. Chen are with the Department of Electronic Engineering, Shanghai Jiao Tong University, Shanghai 201210, China (e-mail: qingqingwu@sjtu.edu.cn; wenchen@sjtu.edu.cn). M. Hua is with the Department of Electrical and Electronic Engineering, Imperial College London, London SW7 2AZ, UK (e-mail: m.hua@imperial.ac.uk). W. Hao is with the School of Electrical and Information Engineering, Zhengzhou University, Zhengzhou 450001, China (e-mail: iewmhao@zzu.edu.cn). M. Jian is with ZTE Corporation, Shenzhen 518057, China (e-mail: jian.mengnan@zte.com.cn).

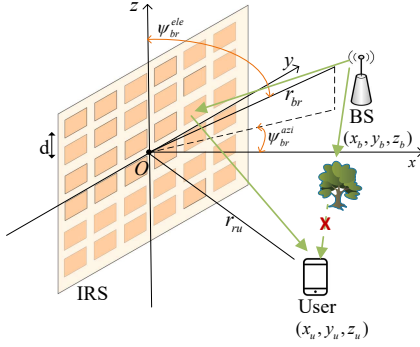


Fig. 1. An IRS-aided THz communication system.

II. SYSTEM MODEL

We consider an IRS-aided THz communication system, where an IRS is deployed to assist the downlink transmission from the BS to a user. In this letter, we focus on the beam split issue at the IRS, thus the BS and the user are assumed equipped with single antenna. Both of them are assumed to be within the Fraunhofer distance of the IRS, i.e., $R = \frac{2D^2}{\lambda_c}$, where D is the maximum aperture of the IRS and λ_c denotes the corresponding signal wavelength. As shown in Fig. 1, we assume that the IRS is located on the $y-z$ plane and centered at the origin in the Cartesian coordinates, which has N_y elements along the y -axis and N_z elements along the z -axis, satisfying $N = N_y \times N_z$. The IRS elements are assumed to be separated by d . Then, the coordinate of the (n_y, n_z) -th IRS element, with $n_y = \{1, \dots, N_y\}$ and $n_z = \{1, \dots, N_z\}$, is given by $(0, \Delta_{n_y}^{N_y} d, \Delta_{n_z}^{N_z} d)$, where $\Delta_a^b = a - \frac{b-1}{2}$, with $a = \{0, \dots, b-1\}$ and $b = \{N_y, N_z\}$. The coordinate of BS is (x_b, y_b, z_b) and that of user is (x_u, y_u, z_u) . The center frequency is denoted by f_c and the bandwidth is denoted by B , which is equally divided into M subcarriers. Then, each subcarrier frequency can be denoted by $f_m = f_c + \frac{B}{M} (m - 1 - \frac{M-1}{2})$, with $\{m = 0, 1, \dots, M-1\}$.

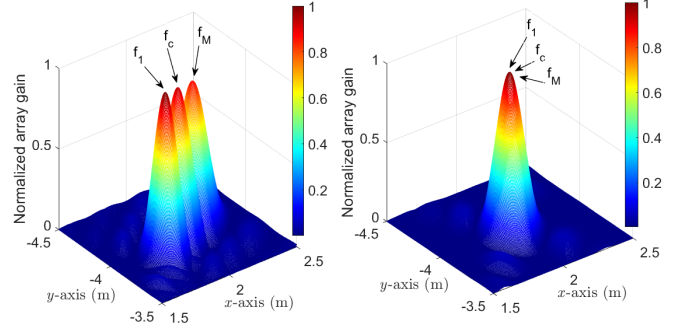
Assuming that the direct link between the BS and the user is blocked by obstructions, the user can only receive signals that are reflected by the IRS. In the THz band, the power gains associated with scattering paths are notably lower compared to the direct line-of-sight (LoS) path, thus we only focus on the LoS channel [7]. The LoS near-field channel between the BS and the IRS at the m -th subcarrier is denoted by $\mathbf{g}_m \in \mathbb{C}^{N \times 1}$, whose entries are given by

$$[\mathbf{g}_m]_{n_y, n_z} = \frac{\alpha_m}{r_{n_y, n_z}^{br}} e^{-j2\pi \frac{f_m}{c} r_{n_y, n_z}^{br}}, \quad (1)$$

where $\frac{\alpha_m}{r_{n_y, n_z}^{br}} = \frac{c}{4\pi f_m r_{n_y, n_z}^{br}}$ denotes the free-space path loss and r_{n_y, n_z}^{br} denotes the distance between the BS and the (n_y, n_z) -th IRS element, which can be written as $r_{n_y, n_z}^{br} = \left(x_b^2 + \left(y_b - \Delta_{n_y}^{N_y} d \right)^2 + \left(z_b - \Delta_{n_z}^{N_z} d \right)^2 \right)^{\frac{1}{2}}$.

Similarly, the LoS near-field channel between the IRS and the user at the m -th subcarrier is denoted as $\mathbf{h}_m \in \mathbb{C}^{N \times 1}$, whose entries are given by

$$[\mathbf{h}_m]_{n_y, n_z} = \frac{\alpha_m}{r_{n_y, n_z}^{ru}} e^{-j2\pi \frac{f_m}{c} r_{n_y, n_z}^{ru}}, \quad (2)$$



(a) Near-field beam split by conventional beamforming. (b) The beams generated by the proposed beamforming design.

Fig. 2. The IRS reflected beams under different cases.

where $r_{n_y, n_z}^{ru} = \left(x_u^2 + \left(y_u - \Delta_{n_y}^{N_y} d \right)^2 + \left(z_u - \Delta_{n_z}^{N_z} d \right)^2 \right)^{\frac{1}{2}}$ represents the distance between the (n_y, n_z) -th IRS element and the user. The IRS reflection coefficients matrix is expressed as

$$\Theta = \text{diag}(\boldsymbol{\theta}) = \text{diag} \left([e^{j\theta_1}, e^{j\theta_2}, \dots, e^{j\theta_N}]^T \right), \quad (3)$$

where $\theta_n \in [0, 2\pi)$, $n = \{1, \dots, N\}$, is the phase shift of the n -th IRS reflecting element [2].

A. Near-field Beam Split Effect at the IRS

We define the normalized array gain of the IRS at the m -th subcarrier as

$$\eta(f_m) = \frac{1}{N} \left| \sum_{n_y=1}^{N_y} \sum_{n_z=1}^{N_z} e^{-j2\pi \frac{f_m}{c} (r_{n_y, n_z}^{br} - r_{n_y, n_z}^{ru})} e^{j\theta_{n_y, n_z}} \right|. \quad (4)$$

The conventional narrowband IRS beamforming design aims at generating the reflected beams towards the target location. We adopt such an IRS beamforming vector based on f_c , expressed as

$$\theta_{n_y, n_z} = \frac{2\pi}{\lambda_c} (r_{n_y, n_z}^{br} - r_{n_y, n_z}^{ru}), \quad \forall n_y, n_z. \quad (5)$$

Owing to the frequency-independent characteristic of (5), the generated beams cannot perfectly point towards the target location in the whole bandwidth, which leads to severe gain loss. In Fig. 2(a), we illustrate this by plotting the normalized array gain at f_c and two edge subcarriers, f_1 and f_M , achieved by (5), under the same setup that will be specified in Section IV. It can be seen that the near-field beam split causes the beams at different subcarriers to split towards different locations. This restricts the user to receive signals that are only around the center frequency.

B. Piece-wise Far-Field Channel Modeling for UPA IRS

We group the adjacent elements of the IRS into a sub-surface that will be imposed by one common TD value. It is assumed that each sub-surface contains $S \times S$ elements, satisfying $S = N_y/K_y = N_z/K_z$. Thus, the number of sub-surfaces is $K = K_y \times K_z$. The coordinate of the center of (k_y, k_z) -th sub-surface, with $k_y = \{1, \dots, K_y\}$ and $k_z =$

$\{1, \dots, K_z\}$, is then given as $(0, \Delta_{k_y}^{K_y} Sd, \Delta_{k_z}^{K_z} Sd)$. Inspired by the piece-wise far-field channel model in [11], we next derive the channel model for the considered UPA-structured IRS. Specifically, by dividing the entire IRS into multiple sub-surfaces, each of which contains much fewer elements compared to the original surface. This partition significantly reduces the near-field range for each sub-surface. As a result, even if the BS/user is within the near-field region of the entire IRS, it can be reasonably assumed to be in the far-field region of each individual sub-surface. Let r_{br} be the distance between the center of IRS and the BS, which can be written as $r_{br} = \sqrt{x_b^2 + y_b^2 + z_b^2}$. Then, the distance between the center of (k_y, k_z) -th sub-surface can be written as

$$\begin{aligned} r_{k_y, k_z}^{br} &= \sqrt{x_b^2 + (y_b - \Delta_{k_y}^{K_y} Sd)^2 + (z_b - \Delta_{k_z}^{K_z} Sd)^2} \\ &= \left(r_{br}^2 + (\Delta_{k_y}^{K_y} Sd)^2 - 2\Delta_{k_y}^{K_y} Sd r_{br} \sin(\psi_{br}^{ele}) \sin(\psi_{br}^{azi}) \right. \\ &\quad \left. + (\Delta_{k_z}^{K_z} Sd)^2 - 2\Delta_{k_z}^{K_z} Sd r_{br} \cos(\psi_{br}^{ele}) \right)^{\frac{1}{2}}. \end{aligned} \quad (6)$$

To this end, the distance $r_{s_y, s_z}^{k_y, k_z}$ between the (s_y, s_z) -th element, with $s_y, s_z = \{1, \dots, S\}$, of the (k_y, k_z) -th sub-surface and the BS can be expressed as

$$\begin{aligned} r_{s_y, s_z}^{br, k_y, k_z} &= \left(r_{k_y, k_z}^{br 2} + (\Delta_{s_z}^S d)^2 - 2\Delta_{s_z}^S d r_{k_y, k_z}^{br} \cos(\psi_{br, k_y, k_z}^{ele}) \right. \\ &\quad \left. + (\Delta_{s_y}^S d)^2 - 2\Delta_{s_y}^S d r_{k_y, k_z}^{br} \sin(\psi_{br, k_y, k_z}^{ele}) \sin(\psi_{br, k_y, k_z}^{azi}) \right)^{\frac{1}{2}} \\ &\stackrel{(a)}{\approx} r_{k_y, k_z}^{br} - \Delta_{s_z}^S d r_{k_y, k_z}^{br} \cos(\psi_{br, k_y, k_z}^{ele}) \\ &\quad - \Delta_{s_y}^S d \sin(\psi_{br, k_y, k_z}^{ele}) \sin(\psi_{br, k_y, k_z}^{azi}), \end{aligned} \quad (7)$$

where

$$\sin(\psi_{br, k_y, k_z}^{azi}) = \frac{y_b - \Delta_{k_y}^{K_y} Sd}{\left(x_b^2 + (y_b - \Delta_{k_y}^{K_y} Sd)^2 \right)^{\frac{1}{2}}}, \quad (8)$$

$$\sin(\psi_{br, k_y, k_z}^{ele}) = \frac{\left(x_b^2 + (y_b - \Delta_{k_y}^{K_y} Sd)^2 \right)^{\frac{1}{2}}}{r_{k_y, k_z}^{br}}, \quad (9)$$

and

$$\cos(\psi_{br, k_y, k_z}^{ele}) = \frac{z_b}{r_{k_y, k_z}^{br}}. \quad (10)$$

(a) in (7) holds due to the first-order Taylor expansion $(1+x)^{\frac{1}{2}} \approx 1 + \frac{1}{2}x$ and the ignorance of $(\Delta_{s_y}^S d)^2$ and $(\Delta_{s_z}^S d)^2$. Accordingly, the normalized near-field channel model between the BS and the (s_y, s_z) -th IRS element in the (k_y, k_z) -th sub-surface is approximated as $\tilde{\mathbf{g}}_m$, whose entries are given by

$$\begin{aligned} [\tilde{\mathbf{g}}_m]_{s_y, s_z}^{k_y, k_z} &= e^{-j2\pi \frac{f_m}{c} r_{k_y, k_z}^{br}} e^{j2\pi \frac{f_m}{c} \Delta_{s_z}^S d r_{k_y, k_z}^{br} \cos(\psi_{br, k_y, k_z}^{ele})} \\ &\quad \times e^{j2\pi \frac{f_m}{c} \Delta_{s_y}^S d \sin(\psi_{br, k_y, k_z}^{ele}) \sin(\psi_{br, k_y, k_z}^{azi})}. \end{aligned} \quad (11)$$

Similarly, the normalized near-field channel between the IRS and the user can be approximated as $\tilde{\mathbf{h}}_m$, whose entries are given as

$$[\tilde{\mathbf{h}}_m]_{s_y, s_z}^{k_y, k_z} = e^{-j2\pi \frac{f_m}{c} r_{k_y, k_z}^{ru}} e^{j2\pi \frac{f_m}{c} \Delta_{s_z}^S d r_{k_y, k_z}^{ru} \cos(\psi_{ru, k_y, k_z}^{ele})}$$

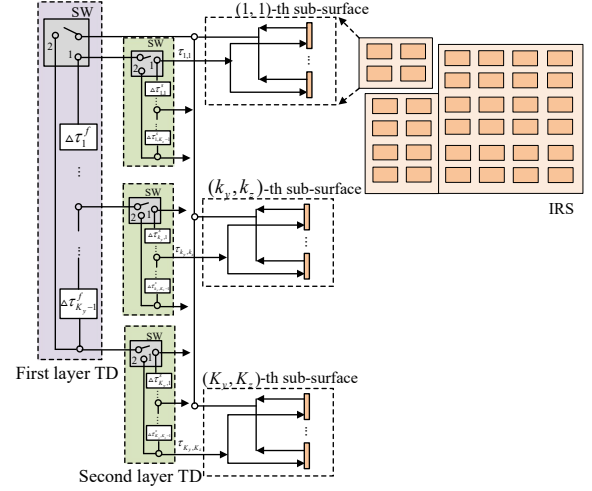


Fig. 3. The proposed DDL IRS beamforming architecture.

$$\times e^{j2\pi \frac{f_m}{c} \Delta_{s_y}^S d \sin(\psi_{ru, k_y, k_z}^{ele}) \sin(\psi_{ru, k_y, k_z}^{azi})}, \quad (12)$$

where the angles are similarly defined as in (8), (9) and (10).

III. PROPOSED IRS BEAMFORMING

In this section, we propose the DLDD IRS beamforming scheme, which enables frequency-dependent IRS beamforming using practical short-range TD modules

Accordingly, the normalized piece-wise far-field cascaded BS-IRS-user channel between the BS and the user, through the reflection of the (s_y, s_z) -th IRS element in the (k_y, k_z) -th sub-surface, can be denoted by $\tilde{\mathbf{b}}_m$, whose entries are given by

$$\begin{aligned} [\tilde{\mathbf{b}}_m]_{s_y, s_z}^{k_y, k_z} &= e^{j2\pi \frac{f_m}{c} (r_{k_y, k_z}^{br} - r_{k_y, k_z}^{ru})} \\ &\quad \times e^{-j2\pi \frac{f_m}{c} (\varphi_{s_y, s_z}^{br, k_y, k_z} - \varphi_{s_y, s_z}^{ru, k_y, k_z})}, \end{aligned} \quad (13)$$

where

$$\begin{aligned} \varphi_{s_y, s_z}^{br, k_y, k_z} &= \Delta_{s_y}^S d \sin(\psi_{br, k_y, k_z}^{ele}) \sin(\psi_{br, k_y, k_z}^{azi}) \\ &\quad + \Delta_{s_z}^S d r_{k_y, k_z}^{br} \cos(\psi_{br, k_y, k_z}^{ele}) \end{aligned} \quad (14)$$

and

$$\begin{aligned} \varphi_{s_y, s_z}^{ru, k_y, k_z} &= \Delta_{s_y}^S d \sin(\psi_{ru, k_y, k_z}^{ele}) \sin(\psi_{ru, k_y, k_z}^{azi}) \\ &\quad + \Delta_{s_z}^S d r_{k_y, k_z}^{ru} \cos(\psi_{ru, k_y, k_z}^{ele}). \end{aligned} \quad (15)$$

The piece-wise far-field channel model makes it straightforward to decouple the phase in (13) into two components: the inter-subsurface phase difference $\Delta_{k_y, k_z}^r = r_{k_y, k_z}^{br} - r_{k_y, k_z}^{ru}$ among different sub-surfaces, and the intra-subsurface phase difference $\Delta\varphi_{s_y, s_z}^{k_y, k_z} = \varphi_{s_y, s_z}^{br, k_y, k_z} - \varphi_{s_y, s_z}^{ru, k_y, k_z}$ within each sub-surface. Considering the fact that each sub-surface contains much fewer elements, this reduces the effect of beam split. Hence, we can reasonably deduce that the intra-surface phase difference $\Delta\varphi_{s_y, s_z}^{k_y, k_z}$ has little effect on the near-field beam split. Thus, we design the TD values to compensate for the inter-surface phase difference Δ_{k_y, k_z}^r in order to alleviate the near-field beam split effect. Accordingly, the required phase shift at the (k_y, k_z) -th sub-surface to combat beam split effect at the m -th subcarrier is given as

$$\vartheta_{k_y, k_z}^m = 2\pi f_m \frac{\Delta_{k_y, k_z}^r}{c}. \quad (16)$$

Consequently, the required delay value is derived by matching the phase shift obtained from a TD module connected to the (k_y, k_z) -th sub-surface to that in (16) as follows

$$\tau_{k_y, k_z} = -\frac{\Delta_{k_y, k_z}^r}{c}, \forall k_y, k_z. \quad (17)$$

However, the delay value can be large in this case. For example, with $\Delta_{k_y, k_z}^r = -3$ meters (m), τ_{k_y, k_z} can be 10000 ps. To avoid excess TD module's limitation, we propose a DLDD architecture as shown in Fig. 3. The first layer TD network utilizes $(K_y - 1)$ TD modules in a step-wise manner, being able to generate K_y cumulative TD values, each of which is connected to a group of $(K_z - 1)$ TD modules in the second layer TD network. Thus, the DLDD architecture contains a total number of $K_t = (K_y - 1) + K_y \times (K_z - 1) = (K - 1)$ TD modules. Specifically, the k_y^t -th delay value, with $k_y^t = \{1, \dots, K_y - 1\}$, in the first layer TD network, is designed to eliminate the phase difference between the $(k_y^t, 1)$ -th and the $(k_y^t + 1, 1)$ -th sub-surfaces, which is given as

$$\Delta\tau_{k_y^t}^f = \tau_{k_y^t+1, 1} - \tau_{k_y^t, 1} = -\frac{\Delta_{k_y^t+1, 1}^r - \Delta_{k_y^t, 1}^r}{c}, \forall k_y^t. \quad (18)$$

Similarly, the k_z^t -th delay value, with $k_z^t = \{1, \dots, K_z - 1\}$, of the k_y -th group in the second layer TD network is designed to eliminate the phase difference between the $(k_y, k_z^t + 1)$ -th and the (k_y, k_z^t) -th sub-surfaces, which is given as

$$\Delta\tau_{k_y, k_z^t}^s = \tau_{k_y, k_z^t+1} - \tau_{k_y, k_z^t} = -\frac{\Delta_{k_y, k_z^t+1}^r - \Delta_{k_y, k_z^t}^r}{c}, \forall k_y, k_z^t. \quad (19)$$

In this way, the delay value applied on the (k_y, k_z) -th sub-surface is realized by a series of TD modules, i.e., $\tau_{k_y, k_z} = \sum_{k=1}^{k_y-1} \Delta\tau_k^f + \sum_{i=1}^{k_z-1} \Delta\tau_{k_y, i}^s$, rather than by a dedicated TD module as in [6]. Through such cumulative TDs, the proposed DLDD IRS beamforming architecture alleviates the maximum delay limitation of TD modules. The TD vector for the first layer TD network is expressed as $\mathbf{t}_f^\Delta = [\Delta\tau_1^f, \dots, \Delta\tau_{K_y-1}^f]$, and that for the second layer TD network is expressed as $\mathbf{t}_s^\Delta = [\Delta\tau_{1,1}^s, \Delta\tau_{1,2}^s, \dots, \Delta\tau_{K_y, K_z-1}^s]$. As demonstrated in (18) and (19), the TD values can be either positive or negative. However, TD modules are unable to generate negative delays. Fortunately, we have the following proposition.

Proposition 1: The sign of $\tau_{k_y, k_z}, \forall k_y, k_z$ is consistent, and the same holds true for $\Delta\tau_{k_y^t}^f, \forall k_y^t$ and $\Delta\tau_{k_y, k_z^t}^s, \forall k_y, k_z^t$.

Proof: It is proved that the IRS needs to be deployed near the BS or the user for optimal performance [12], which yields $r_{br} \gg r_{ru}$ or $r_{br} \ll r_{ru}$. It is intuitive that, in either case, the sign of $\tau_{k_y, k_z}, \forall k_y, k_z$ is consistent. Taking $r_{br} \ll r_{ru}$ as an example, as k_y increases, it is obvious that the increase in r_{k_y, k_z}^{br} is more significant than that in r_{k_y, k_z}^{ru} , which results in negative sign of $\Delta\tau_{k_y^t}^f, \forall k_y^t$, and vice versa. The consistency of the sign of $\Delta\tau_{k_y, k_z^t}^s, \forall k_y, k_z^t$ can be similarly proved. This completes the proof. \square

Building upon proposition 1, we propose to insert a 2-output switch before each group of TD modules. The switch closes its 1st output when the elements of \mathbf{t}_f^Δ or \mathbf{t}_s^Δ are positive,

or rather directs the signal through the 2nd output to the TD network.

On the other hand, the IRS phase shift is designed to align with the intra-surface phase discrepancy $\Delta\varphi_{s_y, s_z}^{k_y, k_z}$. Specifically, for the (s_y, s_z) -th IRS element in the (k_y, k_z) -th sub-surface, we have

$$\theta_{s_y, s_z}^{k_y, k_z} = \text{mod} \left(2\pi \frac{f_c}{c} \Delta\varphi_{s_y, s_z}^{k_y, k_z}, 2\pi \right), \forall k_y, k_z, s_y, s_z, \quad (20)$$

where mod is the modulo operation. To this end, the design of the proposed DLDD IRS beamforming scheme is achieved by (18), (19) and (20).

IV. NUMERICAL RESULTS

In this section, numerical results are presented to illustrate the effectiveness of the proposed DLDD IRS beamforming scheme. The center of the IRS is located at $(0, 0, 0)$ m of a three-dimensional coordinate system. The BS and the user are located at $(0, 1.5, -1.5)$ m and $(2, -4, -2)$, respectively. It is assumed the IRS elements are separated by half of the wavelength, i.e., $d = \frac{\lambda_c}{2}$. Without otherwise specified, the parameters are set as: $N = 100 \times 100$, $K = 10 \times 10$, $f_c = 300$, $B = 30$, and $M = 128$. For comparison, the optimal frequency-dependent IRS beamforming serves as the performance upper bound, where each element is equipped with a TD module [8], and the conventional IRS beamforming without TD modules is adopted as benchmark.

The generated beams at the center frequency, f_c , and the edge subcarriers, f_1 and f_M , by adopting the proposed DLDD IRS beamforming scheme are presented in Fig. 2(b). By comparing Fig. 2(a) and (b), it is observed that the proposed scheme can focus the generated beams at different frequencies to the target location. The normalized array gains at different subcarriers are further illustrated in Fig. 4(a). It can be seen that the near-field beam split effect of IRS is suppressed by our proposed scheme. Specifically, in the wideband system with $B = 30$ GHz, the normalized array gain of conventional narrowband IRS beamforming suffers over 90% loss at the edge subcarriers, as compared to the narrowband case with $B = 0.3$ GHz. By performing the proposed DLDD IRS beamforming scheme, the array gain loss can be effectively reduced to about 2%. Put differently, the proposed scheme can achieve up to 98% near-optimal array gain across the entire bandwidth. Therefore, it can effectively serve as a wideband IRS beamforming design.

Fig. 4(b) shows the normalized edge subcarrier array gain versus the number of TD modules, K_t . We can see that even a small number of TD modules, e.g., $K_t = 24$, readily achieves a good performance at edge subcarrier. Therefore, different strategies can be employed under different scenarios. For example, in the case of beam sweep, the angle spread is advantageous as it accelerates the process, whereas the TD modules may not be favorable. However, during data transmission in a large IRS-aided wideband communication system, the angle spread caused by the beam split is undesirable. This is because it significantly reduces the array gain at the edge frequencies compared to the center frequency. In this case, employing TD module is a favorable choice, and the

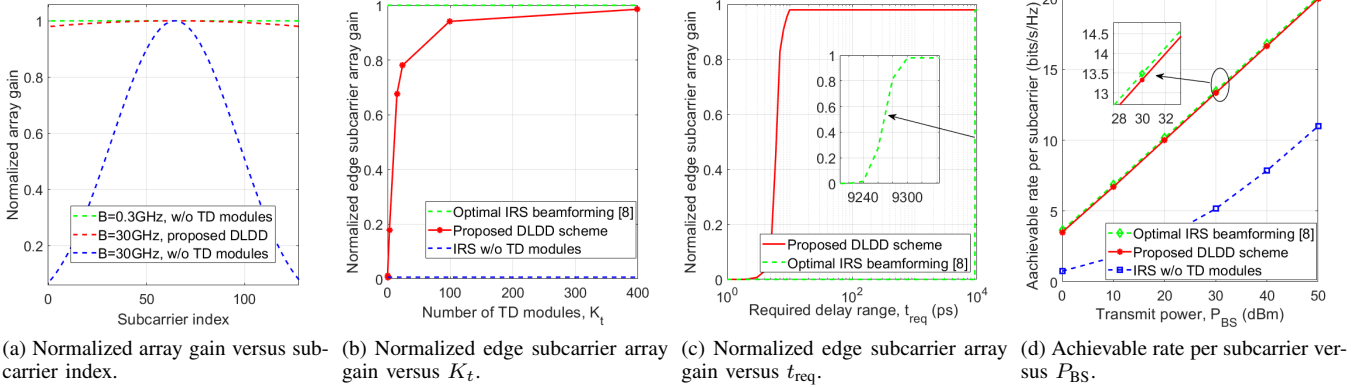


Fig. 4. Simulation results.

proposed method can effectively reduce the required number of TD modules, which remarkably reduces the hardware cost and power consumption of the system.

Fig. 4(c) illustrates the normalized edge subcarrier array gain versus the required delay range, t_{req} . It is observed that the normalized edge subcarrier array gains of both schemes increase as t_{req} scales up, as expected. However, the edge subcarrier array gain loss of the optimal solution proposed in [8] is large until t_{max} is sufficiently large as mentioned in Section III, which is hard to realize in practice. In contrast, the proposed scheme achieves a normalized edge subcarrier array gain of 0.95 for $t_{req} = 9$ ps. This significant improvement comes from the DLDD IRS beamforming design, as it does not require the delay range to increase with distance.

In Fig. 4(d), the achievable rate per subcarrier versus BS transmit power, P_{BS} , is provided. It is observed that the proposed scheme increases the achievable rate by about 110% as compared to the narrowband design. Moreover, it approaches the optimal performance with a performance loss of less than 2%. Such slight performance loss arises from the design of the first layer TD network in eq. (18) as the phase difference between adjacent sub-surface along y -axis varies with different values of k_z . Nonetheless, the proposed scheme still achieves a near-optimal performance, which again reveals its superiority in alleviating the near-field beam split at the IRS.

V. CONCLUSION

In this letter, we proposed a novel wideband beamforming architecture that addresses the near-field beam split effect for the IRS-aided THz communication system. Initially, the near-field beam split effect was analyzed, which revealed that the beams at different frequencies point towards different locations. To address this issue, we extended the piece-wise far-field model to the UPA-structured IRS, based on which, a DLDD IRS beamforming architecture was proposed. Simulation results demonstrated that the proposed DLDD IRS beamforming scheme can mitigate the near-field beam split effect and achieve a near-optimal performance with lower hardware cost. Notably, it showed that the maximum delay range required for TD modules is significantly reduced compared to the state-of-art delay-based architecture.

REFERENCES

- [1] W. Hao *et al.*, "Ultra wideband THz IRS communications: Applications, challenges, key techniques, and research opportunities," *IEEE Network*, vol. 36, no. 6, pp. 214–220, Nov./Dec. 2022.
- [2] Q. Wu and R. Zhang, "Intelligent reflecting surface enhanced wireless network via joint active and passive beamforming," *IEEE Trans. Wireless Commun.*, vol. 18, no. 11, pp. 5394–5409, Nov. 2019.
- [3] M. Hua *et al.*, "Secure intelligent reflecting surface-aided integrated sensing and communication," *IEEE Trans. Wireless Commun.*, vol. 23, no. 1, pp. 575–591, Jan. 2024.
- [4] B. Ning *et al.*, "Terahertz multi-user massive MIMO with intelligent reflecting surface: Beam training and hybrid beamforming," *IEEE Trans. Vehi. Tech.*, vol. 70, no. 2, pp. 1376–1393, Feb. 2021.
- [5] J. An *et al.*, "Reconfigurable intelligent surface-enhanced OFDM communications via delay adjustable metasurface," 2021. [Online]. Available: <https://arxiv.org/abs/2110.09291>
- [6] H. Sun *et al.*, "Time-delay unit based beam squint mitigation for RIS-aided communications," *IEEE Commun. Lett.*, vol. 26, no. 9, pp. 2220–2224, Jun. 2022.
- [7] R. Su, L. Dai, and D. W. K. Ng, "Wideband precoding for RIS-aided THz communications," *IEEE Trans. Commun.*, vol. 71, no. 6, pp. 3592–3604, Jun. 2023.
- [8] W. Hao *et al.*, "The far-/near-field beam squint and solutions for THz intelligent reflecting surface communications," *IEEE Trans. Vehi. Tech.*, vol. 72, no. 8, pp. 10 107–10 118, Mar. 2023.
- [9] A. Karakuzulu *et al.*, "Broadband 110–170 GHz true time delay circuit in a 130-nm SiGe BiCMOS technology," in *2020 IEEE/MTT-S Int. Microwave Symposium (IMS)*, Aug. 2020, pp. 775–778.
- [10] A. Najjar *et al.*, "Hybrid delay-phase precoding in wideband UM-MIMO systems under true time delay and phase shifter hardware limitations," *IEEE Trans. Wireless Commun.*, vol. 23, no. 7, pp. 7246–7262, Jul. 2024.
- [11] M. Cui and L. Dai, "Near-field wideband beamforming for extremely large antenna arrays," *IEEE Trans. Wireless Commun.*, 2024, early access, doi: 10.1109/TWC.2024.3398770.
- [12] Q. Wu *et al.*, "Intelligent reflecting surface-aided wireless communications: A tutorial," *IEEE Trans. Commun.*, vol. 69, no. 5, pp. 3313–3351, May 2021.